Ceramics International 42 (2016) 11780–11795

Contents lists available at ScienceDirect

Ceramics International

journal homepage: www.elsevier.com/locate/ceramint

Conductivity and dielectric properties of $SrLa_xBi_xY_xFe_{12-3x}O_{19}$ $(0.0 \leq x \leq 0.33)$ hexaferrites

Y. Bakış [a], I.A. Auwal [b], B. Ünal [c], A. Baykal [b,*]

[a] Department of Bio and Nano Technology Engineering, Faith University, B.Çekmece, 34500 Istanbul, Turkey
[b] Department of Chemistry, Fatih University, B.Çekmece, 34500 Istanbul, Turkey
[c] Department of Software Engineering, Istanbul Sabahattin Zaim University, Halkali Cad., K.Çekmece, 34303 Istanbul, Turkey

ARTICLE INFO

Article history:
Received 8 April 2016
Received in revised form
14 April 2016
Accepted 19 April 2016
Available online 20 April 2016

Keywords:
Hexaferrites
Electrical conductivity
Dielectric constant
Dielectric loss
Resistivity

ABSTRACT

Both Y-La-Bi substituted and non-substituted Sr-hexaferrites (SrM) were synthesized by sol-gel auto combustion technique and the influences of Y, La and Bi ions on ac/dc conductivities, dielectric constant/loss properties as well as complex dielectric modulus were investigated extensively for a variety of substitutions. It was observed that ac conductivity of SrM increases slightly with increasing Y^{3+} La^{3}, and Bi^{3+} substitutions at first, and then decreases with its further increments. Furthermore, ac conductivity increased with increasing frequency which could be regarded as an origin indication of both electronic and polaron hopping *mechanism*. It is also worthy to note that the activation energy, which is an indication of both mechanisms depicted in the Arrhenius plot, is increased as the enhanced contributions of substitutions in SrM with the illustration of a better stability and tunability of electrical bonds among *substituted* ions and ferrous and ferric ions. The dielectric constant, dielectric loss and dielectric modulus represent a very interesting tunability and optimised consequences regarding to the variation of frequencies, temperatures and substitutions of SrM.

1. Introduction

Hexagonal ferrites are valuable magnetic materials with multi-applications in technology and good commercial value. The most important class of hexaferrite with an exceptional significance in electronic industries is M-type hexaferrites, ($MFe_{12}O_{19}$, where M can be Ba, Sr or Pb). Pure SrM has been intensively studied [1–4] owing to its amazing magneto-electrical properties such as large values of saturation magnetization, coercivity, curie temperature and excellent high-frequency response with low loss, they are currently used in microwave devices operating in GHz range frequency, magnetic recording media, materials for permanent magnets, and in electronic machines [5].

Recently, researchers are keen on synthesis and characterization of several derivatives of SrM through different synthesis approaches [6–9]. This is because when Fe or Sr is partially replaced with different cations of relatively similar ionic radius, a material with new properties is formed. The mechanism of electrical conductivity of M-type hexaferrite can simply be explained on the basis of the association of Fe^{2+} with Fe^{3+}, situated at the adjacent octahedral site. This effect leads to low resistivity as an interchange ("hopping") of electrons can take place very readily, producing current [5,10,11]. At room temperature, the conduction of ferrites is as result of impurities, however the conduction at high temperature is due to polaron hopping [12].

Materials with high electrical resistivity and low eddy current are most suitable for microwave application [13]. Alange et al. [14] synthesized Al-Cr BaM with formula $BaCr_xAl_xFe_{12-2x}O_{19}$ using sol gel auto combustion method and the result shows the dielectric properties dependence on frequency and doping concentration. As frequency increases, the dielectric constant (ε'), dielectric loss (ε'') and dielectric loss tangent (δ) all decreases rapidly, the observed effect was ascribed to Maxwell-Wangner polarization and conduction mechanism. Azim et al. [15] incorporated La^{3+} in SrM. Their study of dielectric property as a function of composition and frequency (100 Hz to 1 MHz) at RT revealed that, ε' decreases drastically as frequency increase and then becomes independent at elevated frequencies. The behavior of ε' was described to be due to dielectric relaxation. The material was evidenced to be a good semiconductor. Moreover, in our previous research [10], simultaneous substitution of Bi^{3+} and La^{3+} in SrM lead to optimization of electrical resistivity, dielectric constant and dielectric loss. Consequently, a good electrical insulator material was formed.

In this study, we performed partial substitution of Fe^{3+} by Y^{3+}, La^{3+} and Bi^{3+} in SrM complex with nominal composition $SrY_xLa_xBi_xFe_{12-3x}O_{19}$ $(0.0 \leq x \leq 0.33)$. Our aim is to find out the

* Corresponding author.
E-mail address: hbaykal@fatih.edu.tr (A. Baykal).

http://dx.doi.org/10.1016/j.ceramint.2016.04.099
0272-8842/

Table 1
Stoichiometric amounts of reactants (in g) for each composition.

Composition (x)	Fe $(NO_3)_3$	Sr $(NO)_2$	Bi_2O_3	La_2O_3	Y_2O_3
0.0	4.848	0.211	–	–	–
0.10	4.726	0.211	0.023	0.016	0.011
0.20	4.605	0.211	0.047	0.032	0.022
0.33	4.444	0.211	0.078	0.055	0.037

effect of these ions on ac and dc conductivity of the ferrite.

2. Experimental

2.1. Intrumentation

The dielectric constant (ε') and dielectric loss (ε'') of a complex dielectric permittivity $\varepsilon^* = [\varepsilon'(\omega) + i\varepsilon''(\omega)]$ and ac–dc conductivities were recorded with a Novocontrol dielectric-impedance analyzer. The dielectric data (ε', ε'') were collected during heating as a function of frequency. The films were sandwiched between gold blocking electrodes and the conductivities were measured in the frequency range 0.1 Hz to 3 MHz at 10 °C intervals. The temperature was controlled with a Novocontrol cryosystem, which is applicable between 20 and 120 °C at an interval of 20 °C.

2.2. Procedure

Highly purity reagents were used in the synthesis, which are all purchased from *Merck* and applied directly without purification step. Sol gel auto combustion technique was employed to prepare $SrY_xLa_xBi_xFe_{12-3x}O_{19}$ $(0.0 \le x \le 0.33)$. To prepare each sample composition, required stoichiometric moles of $(Sr(NO_3)_2$, iron (III) nitrate $(FeNO_3)_3 \cdot 6H_2O$, La_2O_3, Y_2O_3 and citric acid (Table 1) were dissolved in small amount of nitric acid before mixing in the complex solution (*because the oxides of La, Bi and Y are not soluble in distilled water*). Citric acid was used as chelating agent as sell *as a fuel to promote combustion process*. The citrate to metal ion ratio was 1:1. The pH was adjusted to reach value of 7 using drops of ammonia solution *in order to have enough free* Ba^{2+} *in the solution*, *which is typically difficult to be chelated then* Fe^{3+}. The solution was evaporated at 80 °C under stirring forming a gel which later combusted *exothermically in to a* light-weight powder. The powder was grounded and heat treated at 1100 °C for 3 h.

3. Results and discussion

3.1. Chemical characterization of products

The complete characterization of all products has been already given our previous publication [16] (Table).

3.2. Impedance spectroscopy

Impedance spectroscopy is an appropriate technique for dealing with the understanding of any submicron sized materials, whose electrical properties over their electronics, dielectrics, and its contributions of any dopants as a type and distribution. The spectroscopic analysis provides some more information with the impedance of submicron-sized grains isolated with grain boundaries [17].

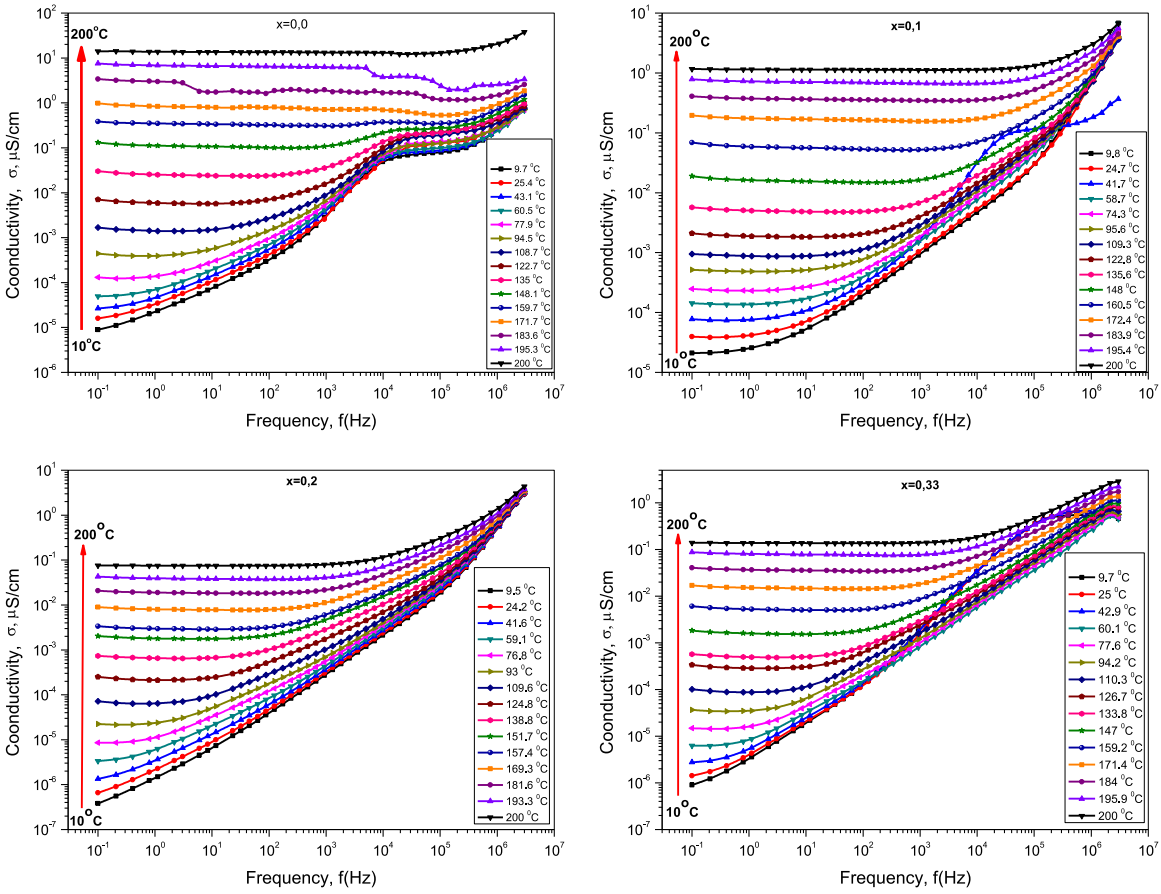

Fig. 1. ac conductivity of Bi-La-Y substituted SrM $(0.0 \le x \le 0.33)$ versus frequencies of up to 3 MHz for temperatures ranging from 10 °C up to 200 °C.

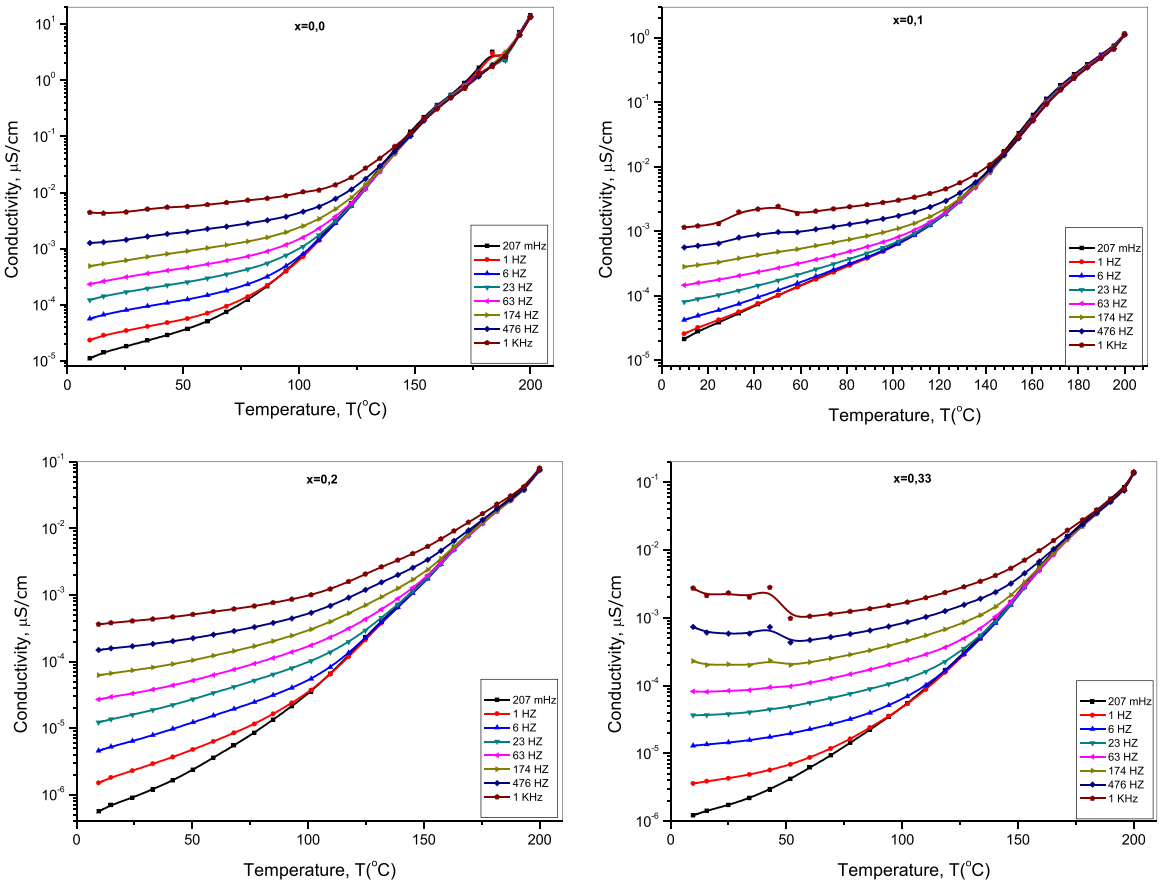

Fig. 2. ac conductivity of Bi-La-Y substituted SrM ($0.0 \leq x \leq 0.33$) versus temperature for lower frequencies up to 1 kHz.

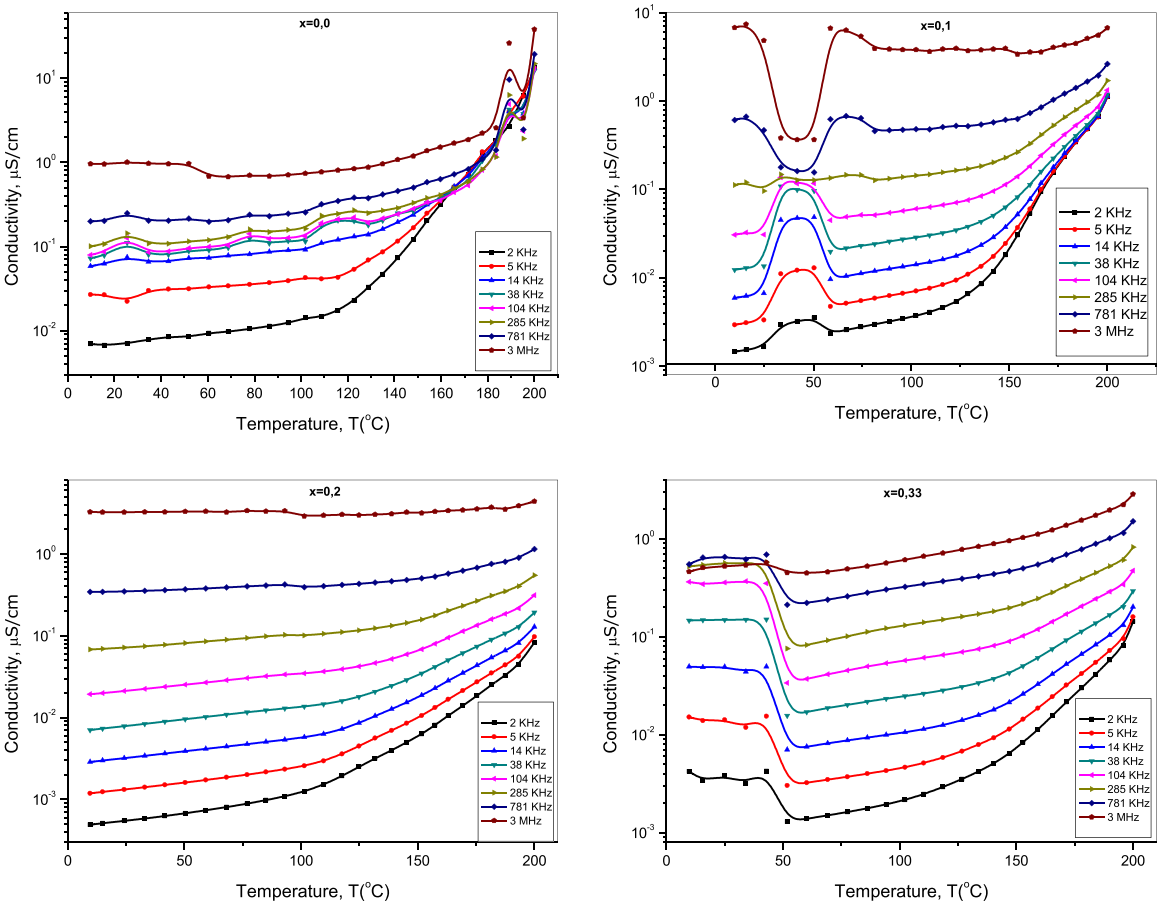

Fig. 3. ac conductivity of Bi-La-Y substituted SrM ($0.0 \leq x \leq 0.33$) versus temperatures for medium and higher frequencies up to 3 MHz.

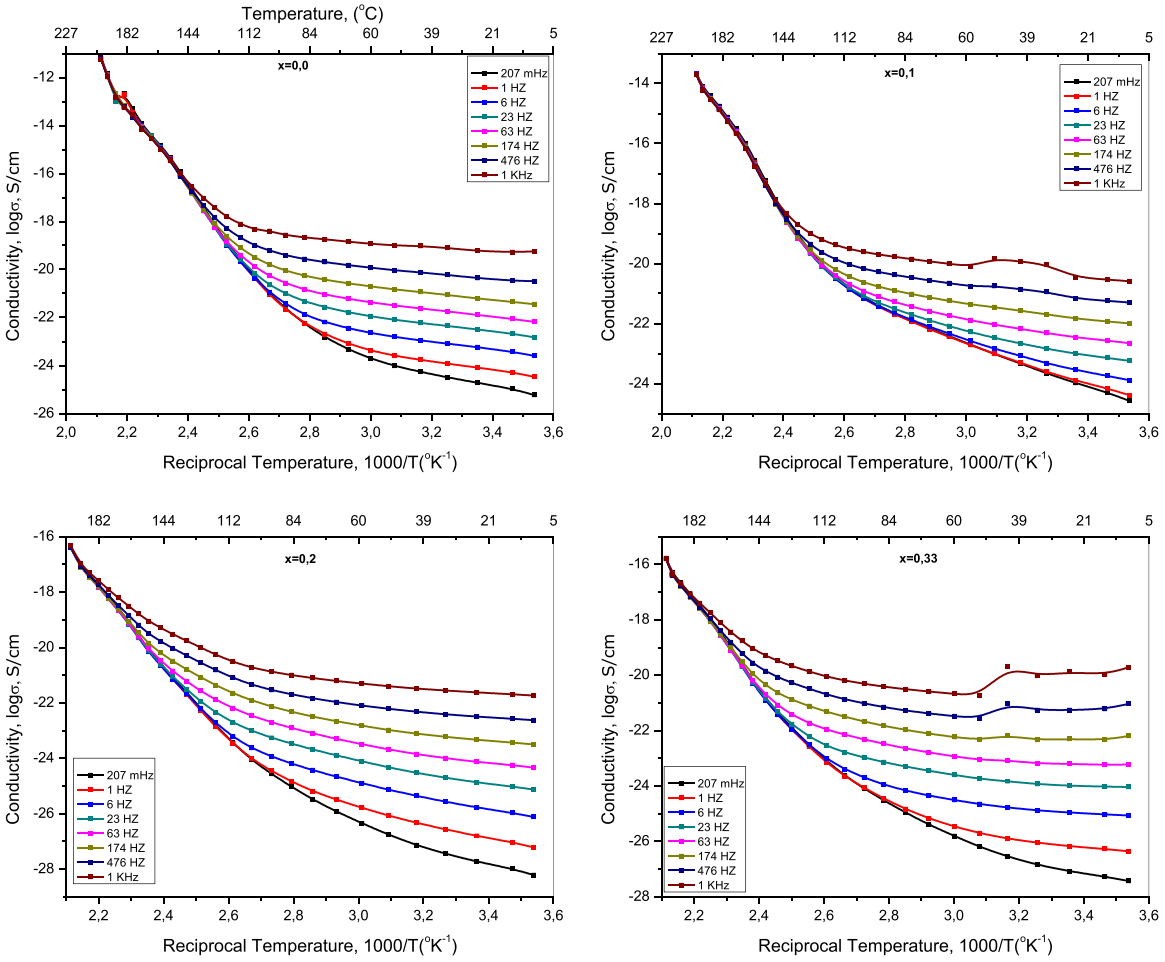

Fig. 4. Conductivity of Bi-La-Y substituted SrM ($0.0 \leq x \leq 0.33$) versus reciprocal temperatures for lower frequencies up to 1 kHz.

3.3. Electrical conductivity and dielectric behavior

The electrical conductivity and dielectric behavior can be explained by any percolated system in various domains for an electrical approach. The response signal to a sinusoidal stimulus is decomposed by Fourier Transformation for the purpose of the evaluation of complex impedance. It is therefore, well-known that the complex dielectric constant is donated by the equation

$$\varepsilon^*(\omega; T) = \varepsilon'(\omega; T) - i\,\varepsilon''(\omega; T) \quad (1)$$

and also complex conductivity is evaluated with an equation of

$$i\sigma^*(\omega; T) = \sigma'(\omega; T) - i\,\sigma''(\omega; T) \quad (2)$$

where $\omega(=2\pi f)$ is the angular frequency of the applied potentials across the coupled electrodes. The *ac* conductivity (σ_{ac}), dielectric constant (ε') and dielectric loss (ε''), tangent ($\tan\delta$) loss can be calculated using a standard relation as follows:

$$\varepsilon' = \frac{Cd}{\varepsilon_0 A} \quad (3)$$

where C is capacitance in Farad (F), A is a cross-sectional area of pellet in m^2, d is the distance across two coupled electrodes and ε_0 ($=8.852 \times 10^{-14}$ F/cm) is the vacuum dielectric permittivity. It is obvious to note that the real component of *ac* conductivity is acquired from the imaginary part of the dielectric loss $\varepsilon''(\omega)$ relative to a formulation of $\epsilon'' = \epsilon' \tan\delta$ and is also summarized as follows;

$$\sigma_{ac} = \omega\varepsilon_0\varepsilon'' = \omega\varepsilon_0\varepsilon' tan\delta \quad (4)$$

where ε" is also termed the imaginary part of complex dielectric permittivity (ε*).

It is recognized that the measurement of frequency-dependency of conductivity is a useful technique to determine transport evolution in a variety of compositional hexaferrites. Overall conductivity is assigned to two components in most of compositional hexaferrites: first part is *dc* conductivity due to "*band conduction*" [18] and second part is *ac* conductivity due to "*hopping mechanism*" between ions of the same element occurring in more than one valence states in which it is represented by a power law dependency with a certain exponent as illustrated in the power law equation in the following section.

All above theoretical overview, the *ac*/*dc* conductivity (σ_{ac}/σ_{dc}), dielectric constant (ϵ') and dielectric loss (ε''), and finally dielectric modulus were evaluated as functions of frequency, composition ($0.0 \leq x \leq 0.33$) and temperature using an impedance analyzer in the frequency range up to 3.0 MHz.

3.4. Conductivity

3.4.1. ac conductivity

The ac conductivity (σ_{ac}) measurements of $SrLa_xBi_xY_xFe_{12-3x}O_{19}$ with $0.0 \leq x \leq 0.33$ were carried out in the range of 10–200 °C using impedance spectroscopy against both frequency and temperature. The frequency-dependency of conductivity for hexaferrites shown in Fig. 1a-d was acquired from the following standard equation [19,20];

$$\sigma'(\omega; T) = \sigma_{ac}(\omega; T) = \varepsilon''(\omega; T)\omega\varepsilon_0 \quad (5)$$

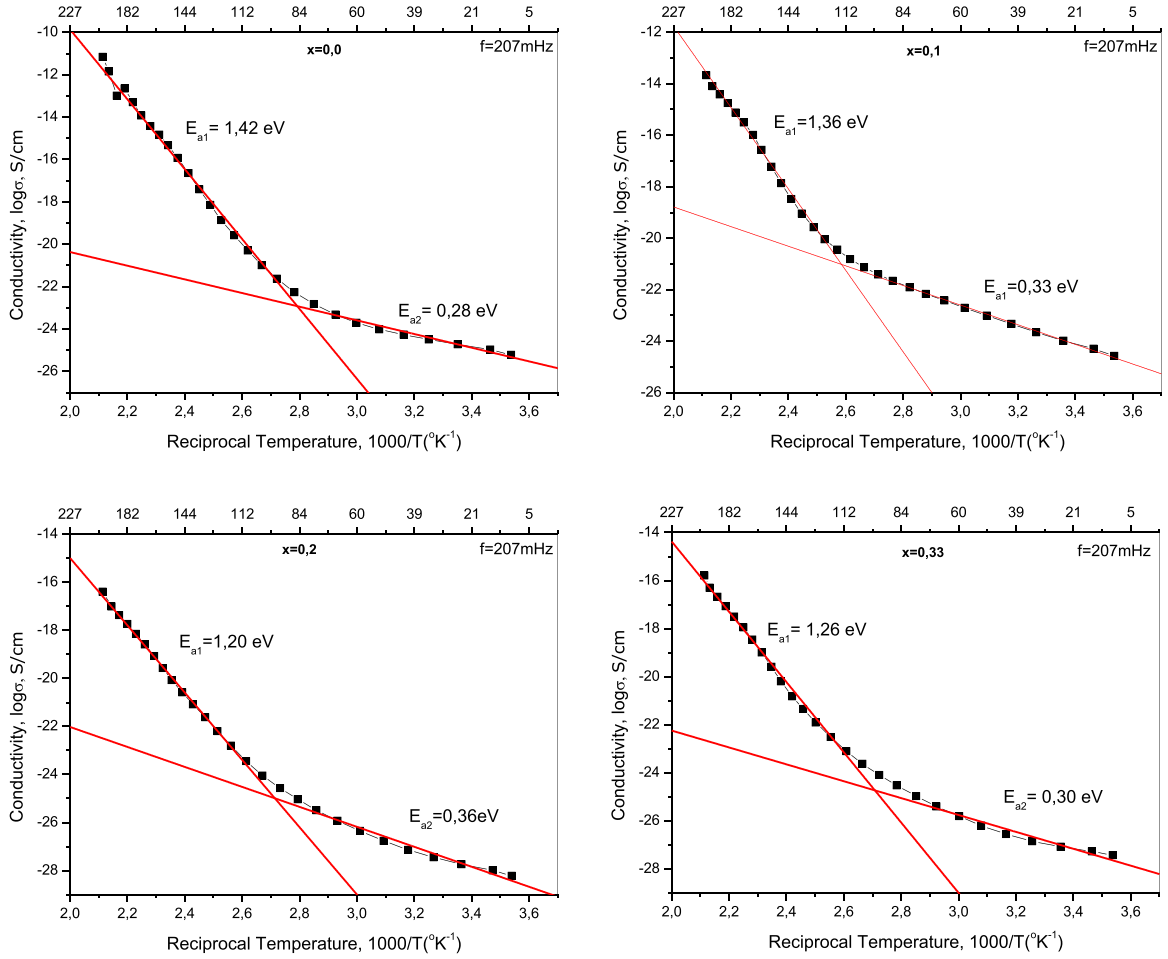

Fig. 5. dc conductivity of Bi-La-Y substituted SrM ($0.0 \leq x \leq 0.33$) versus reciprocal temperatures for just 207 mHz.

where $\sigma'(\omega;T)$ is the real component of complex conductivity, ω (=2πf) is the angular frequency of *ac* signal applied to the sample, ε'' is the imaginary part of complex dielectric permittivity (ε^*) and ε_0 ($=8.852 \times 10^{-14}$ F cm^{-1}) is the vacuum permittivity.

It can be clearly seen from Fig. 1 for all the substitutions that ac conductivity represents a similar tendency for temperatures up to 200 °C, while at lower temperature it can be explained with the power law of an exponent *n*. However, while temperature is increased, the power law rule is converted into valley tendency becoming independent frequency at higher temperatures. It is noted that temperature influence over the conductivity is considerably high and its mechanism should be explained by attributing to the ratio of substitutions. Nevertheless, temperature dependency of conductivity reduces at higher frequencies, say about over 100k Hz depending upon substitutions. As a result, small ratios of dopants of Bi^{3+}, La^{3+} and Y^{3+} ions into ferrites contribute considerable influences to *ac* conductivity. On the other hand, there could also be interesting points at higher concentration, say $x=0.33$, that *ac* conductivity decreases first, and then it increases according to incremental rise of the ratio of the substitution. Furthermore, temperature dependency of the conductivity at higher frequency becomes almost lesser effect for all concentration ratios. It can be clearly seen that in some region of the graphs, *ac* conductivity as functions of both frequency and temperature can be evaluated in the form of a power law as follows;

$$\sigma(\omega;T) = \sigma_{dc} + \sigma_0(T)\omega^n \quad (6)$$

where $\sigma_{dc}(T)$ is *dc* conductivity, and $\sigma_0(T)$ the pre-coefficient of *ac* conductivity with a temperature dependency only, and *n* is the power exponent in slightly dependence with substitutions and temperature as well as some interested region of higher frequency. The power exponent is also a dimensionless quantity taking values between *null* and *unity*, when *null* conduction is *dc* conduction which is frequency-independent, but for $n \leq 1$, the conduction is *ac* conduction. It can be easily calculated from slope of the graphs of $\log\omega$ versus $\log\sigma_{ac}$ for each of the substitutions.

Both Bi-La-Y substituted and non-substituted strontium hexaferrites shows the semiconducting behavior i.e. conductivity increases with temperature in the range of 283–473 K for a value of substitutions less than 0.33. This type of conductivity behavior with temperature has already been reported for M-type strontium hexaferrites [21] and spinel ferrites [22,23]. Any value of transition temperature does not appear with Bi–La and Y content. So, the occurrence of phase transition, cation migration, cation reordering, and the presence of impurities are supposed to be non-dominant within the conductivity temperature mechanism.

It is suggested that conduction phenomenon is ac conduction due to hopping of charge carriers. The conductivity containing Bi^{3+}, La^{3+} and Y^{3+} ions increases with increasing frequency as can be seen in other ferrites in most literatures [24,25] while it is strongly depended upon temperature ranges. All this type of tendencies is considered to be a general dielectric behavior and can be explained on the basis that the *hopping conduction* between ferrous and ferric ions increases at higher frequencies while some charges from different trapping centers are released which support in conduction mechanism by hopping electron conduction. Conductivity decreases with the increase in Bi^{3+}, La^{3+} and Y^{3+}

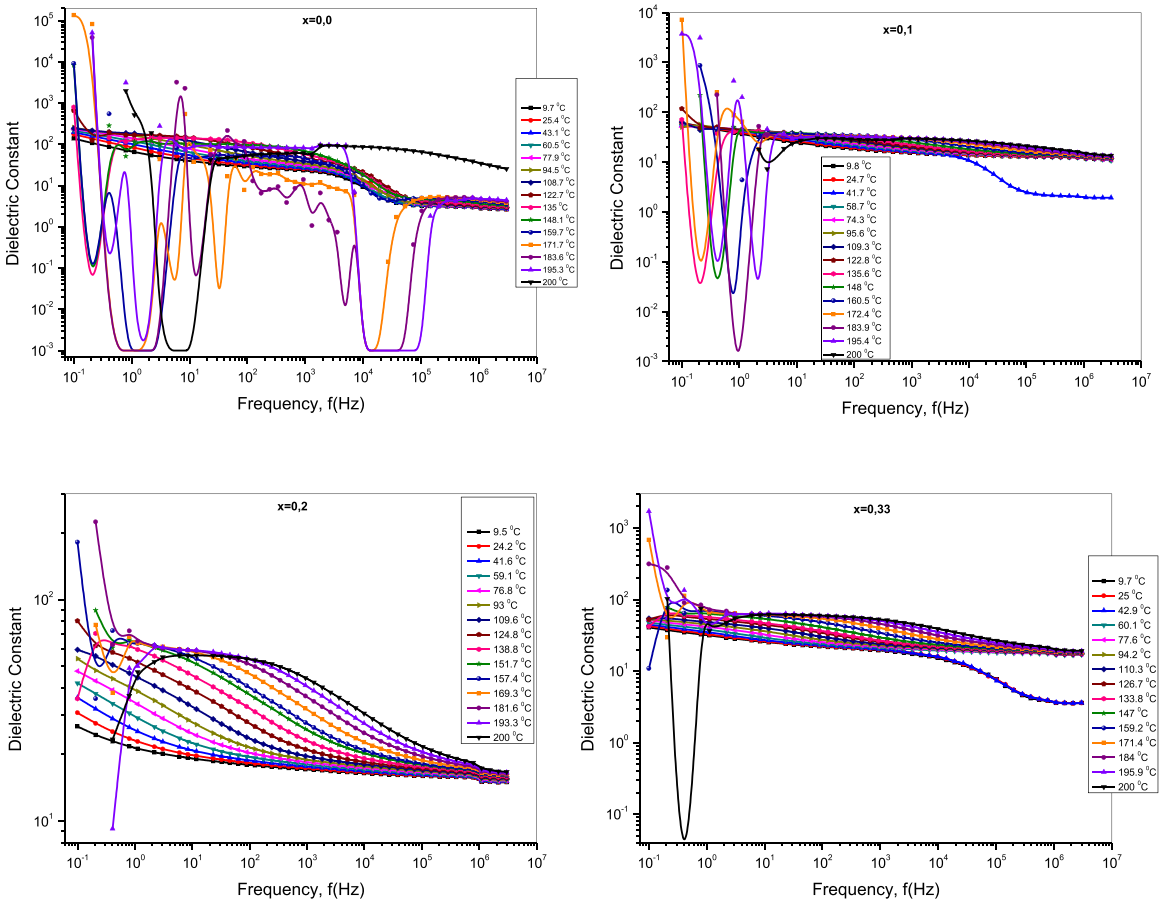

Fig. 6. Dielectric constant of Bi-La-Y substituted SrM ($0.0 \leq x \leq 0.33$) versus frequencies of up to 3 MHz for temperatures ranging from 10 °C up to 200 °C.

ions concentration which may be due to incremental amount of Bi^{3+}, La^{3+} and Y^{3+} ions which do not participate in conduction mechanism, and also restrict the hopping conduction between ferric and ferrous ions, i.e. $Fe^{2+} \leftrightarrow Fe^{3+}$ ions, as Bi^{3+}, La^{3+} and Y^{3+} ions preferentially may reside in octahedral site since similar conduction mechanism is interpreted as in the case of Bi^{3+}, and La^{3+} ions - substituted Fe_3O_4 nano-particles [10,26].

According to Rezlescu model [27,28] the conductivity in ferrites is due to the hopping of electrons between Fe^{3+} and Fe^{2+} at the octahedral sites. The value of conductivity of Bi-La-Y substituted strontium hexaferrites is decreased due to replacement of Fe ions from octahedral sites especially by the substitution of Bi ions for all temperatures up to 200 °C. This reduces the number of Fe ions at octahedral sites, which results in decrease of electron hopping and the number of Fe^{2+} ions thus causing the resistivity to increase. The Bi^{2+} ion occupies the lattice interstitial octahedral B site and distorts the lattice to generate internal stress, which confines the electron hopping and then reduces the Fe^{2+} generation [29,30] Finally, *ac* conductivity (σ_{ac}) was found to decrease with increase in Bi^{3+}, La^{3+} and Y^{3+} ions substitutions, and can be explained on the basis of hopping mechanism. So the hopping conduction can be tuned in some extent by addition of Bi^{3+}, La^{3+} and Y^{3+} ions in ferrites as well.

It can be clearly seen from Fig. 2 that for lower frequency ac conductivity increases with temperature with a power law initially depend on frequency at lower temperature and independent of frequency at higher temperature for a variety of frequency value up to 1 kHz. This temperature dependency is also correlated with the ratio of substitutions. This type of variation can be also attributed to some contribution of '*small polaron hopping*' to the conductivity.

For medium and higher frequency range ac conductivity is rather complicated because of a contribution of both electron and polaron hopping conductions to the conductivity as well as the replacements of the ferric and ferrous ions with the substitution ions. Conduction mechanism seems to be optimised for, and electron hopping contribution is dominated for x=0.2 when compared with others as can be seen from Fig. 3.

3.4.2. *dc conductivity*

The dc electrical conductivities of both $SrLa_xBi_xY_xFe_{12-3x}O_{19}$ ($0.0 \leq x \leq 0.33$) and strontium hexaferrites ($SrFe_{12}O_{19}$) were derived from the well-developed plateau region in graphs of $\log \sigma_{ac}$ versus log*f* by taking the values at 0.207 Hz as shown in Fig. 4 and, furthermore the conductivities of lower frequency dependent versus reciprocal temperature between 10 up to 200 °C are shown in Fig. 5 for each of ferrite ($0.0 \leq x \leq 0.33$). The dc conductivity curve of strontium hexaferrite reveals strongly temperature-dependent behavior and it can be divided into two regions over the temperature range of 10–200 °C involving transition region around 85 °C, However, those of Bi-La-Y substituted SrM reveals intensely temperature-dependent tendencies as well, and it can be divided into two regions over the same temperature range involving transition region around 110 °C for x=0.1 and 95 °C for $x=0.2$ and 0.33. The dc conductivity exhibits Arrhenius behavior before and after transition temperature providing two values of the activation energy as mentioned earlier. It could be indicated that the conductivity of both SrM and Bi-La-Y substituted SrM are thermally activated and it can be explained using the following Arrhenius relation as mentioned earlier.

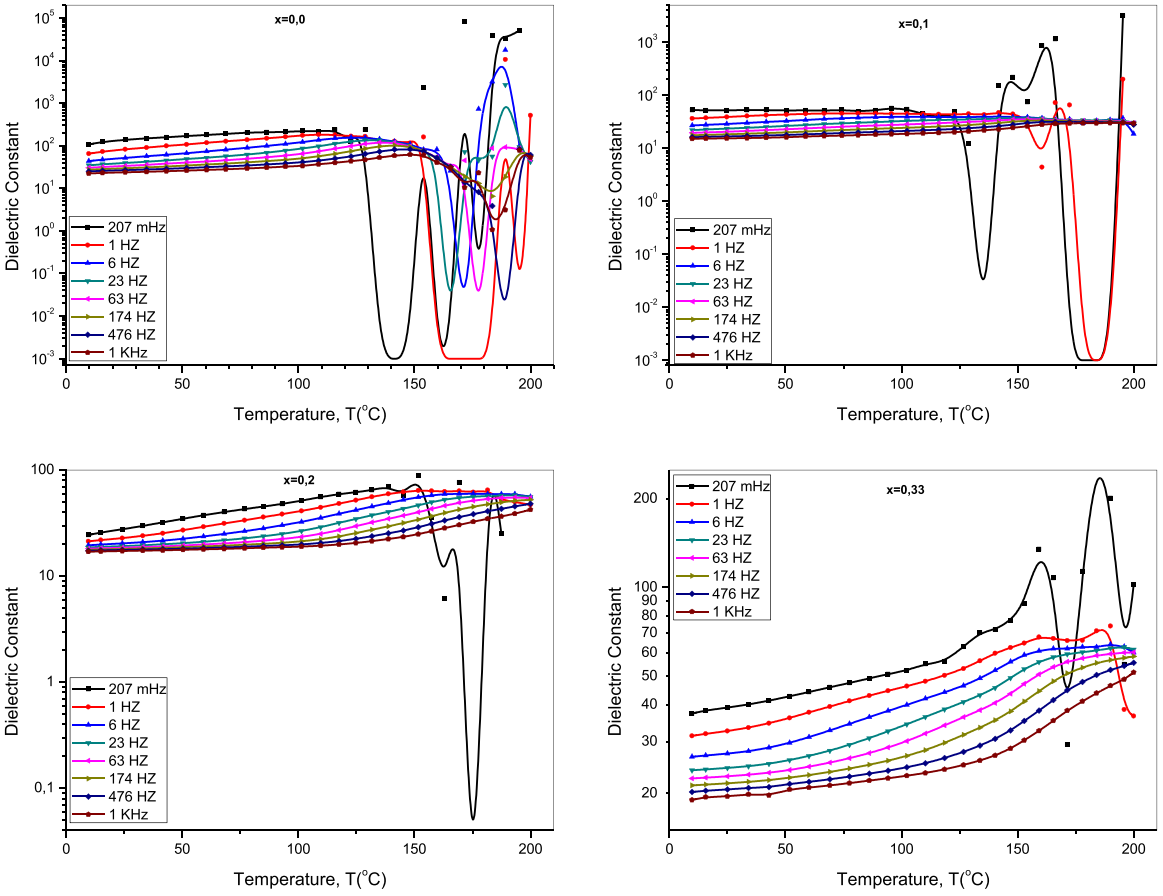

Fig. 7. Dielectric constant of Bi-La-Y substituted SrM ($0.0 \leq x \leq 0.33$) versus temperatures for lower frequencies up to 1 kHz.

$$\sigma_{dc}(T) = \sigma(0)\exp\left[-\frac{E_a}{k_B T}\right] \tag{7}$$

where σ_{dc} is the dc conductivity, $\sigma(0)$ is the pre-exponential term, E_a is the activation energy, k_B is the Boltzmann constant (8.617×10^{-5} eV K^{-1}) and T is the temperature in K. Accordingly, *dc* conductivity can be expressed as an Arrhenius plot for a range of components with a legend depicted in the graphs. Temperature-independent coefficient, $\sigma(0)$, of the conductivity is found to only be dependent upon the content of Bi^{3+}, La^{3+} and Y^{3+} ions in hexaferrites. So the coefficients are calculated to vary up to a few *nS/cm* for non-substituted SrM and up to a few tens *pS/cm* for substituted ones. As a result, conductivity coefficients vary with the content of Bi^{3+}, La^{3+} and Y^{3+} ions whereas the activation energies change roughly into two regions when compared with each other as mentioned earlier.

As can be seen from the first graph of Fig. 5a sample of SrM represents two regions with different activation energies of 1.42 eV and 0.28 eV after and before a transition region of 85 °C, respectively. However, the lower ratio in substitutions shows a remarkable increase in *dc* conductivity, and then further incremental ratio causes to incline conductivity when compared with others in the same condition of measurements. Additionally, the transition temperature shifts to a higher temperature value of 110 °C with substitution of Bi^{3+}, La^{3+} and Y^{3+} ions. Accordingly, relevant activation energies have values of 1.36 eV at higher side of, and 0.33 eV at a lower site of transition temperature. Within a substitution ratio here, activation energy at higher temperature side decreases first, and then increases while at lower side this happens vice versa. Activation energy represents a steady state trend with increasing the substitutions of Bi^{3+}, La^{3+} and Y^{3+} ions which means that more energy is required for charge carriers to jump from one cationic site to another together with increasing substituent ions which causes a decline in *dc* conductivity in some extent depicted in Fig. 5 for all the ferrites studied here.

At higher temperature, *dc* conductivity is observed to decrease on increasing Bi-La-Y substituent since at lower temperature increases with increasing Bi-La-Y substituent. According to Verwey et al. [31,32] the conduction mechanism in ferrites is due to hopping of electrons between Fe^{3+} and Fe^{2+} at octahedral sites. Therefore, the conductivity of the ferrite materials strongly depends up on the site occupation of the substituent. It has been reported that Bi^{3+} replaces the iron at octahedral sites and it also oxidizes to Bi^{5+} for high temperature measurements considering as somehow annealing process [33,34] The Bi^{5+} has preference for tetrahedral sites and enforces the ferric ions from tetrahedral sites to migrate gradually to octahedral sites. As a result, the number of ferric ions increases at the octahedral site as well as hopping of electrons. Consequently, the conductivity starts to increases. Further due to oxidation of Bi^{3+} to Bi^{5+} holes are created which also contribute to conduction. The increases in Fe^{3+} ions at octahedral site as well as the creation of holes are responsible for the reduction in conductivity. For the case of lower temperature, activation energy for all the substituents would be low and conductivity could be attributed both '*electron* and *polaron hopping*' mechanism (*Conduction mechanism in ferrite is due to hopping of electron between* Fe^{2+} *and* Fe^{3+} *ions. Due to increasing hopping between* Fe^{2+} *and* Fe^{3+} *ions at the octahedral* (*B*) *site, there is an increase in the conductivity and therefore the resistivity decreases*). So, the activation energy of both Bi-La-Y substituted and non-substituted SrM is calculated to be less than 400 meV at a lower

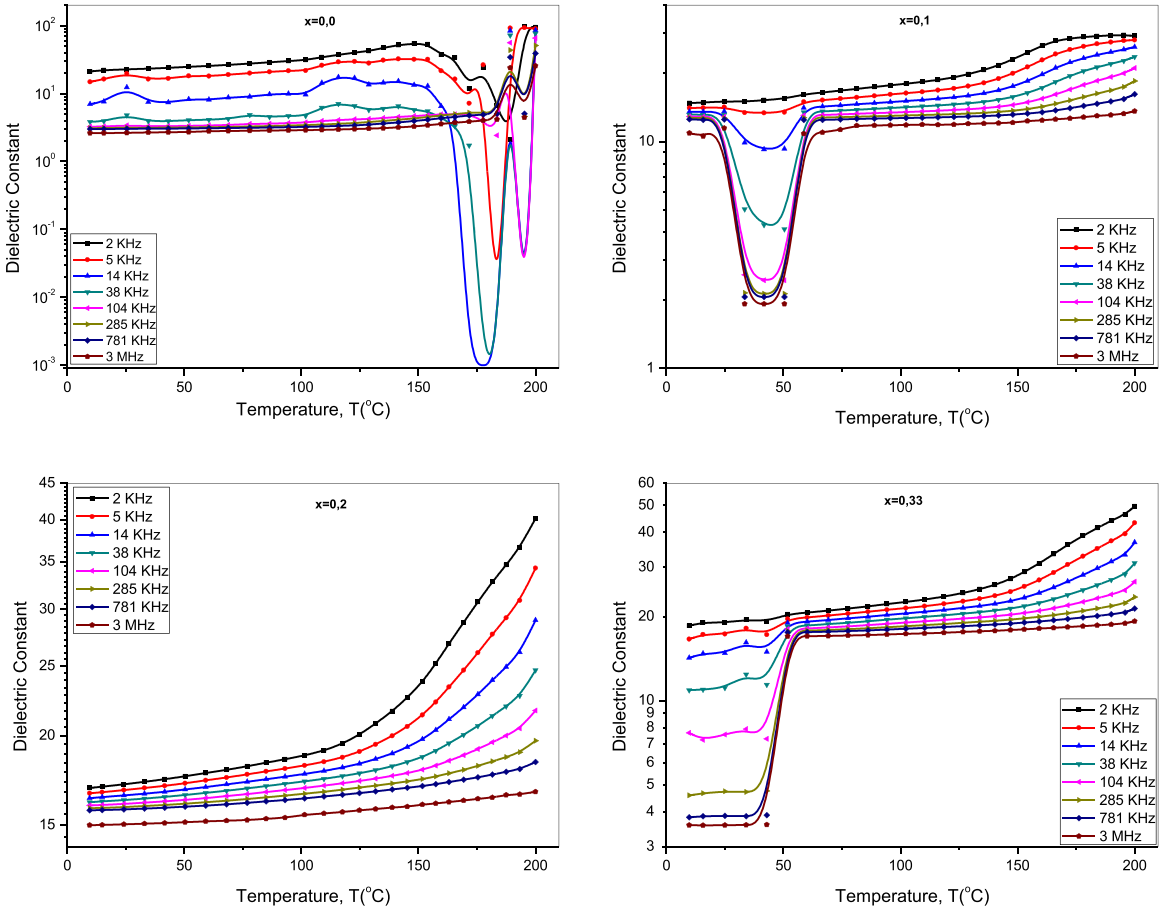

Fig. 8. Dielectric constant of Bi-La-Y substituted SrM ($0.0 \leq x \leq 0.33$) versus temperatures for medium and higher frequencies up to 3 MHz.

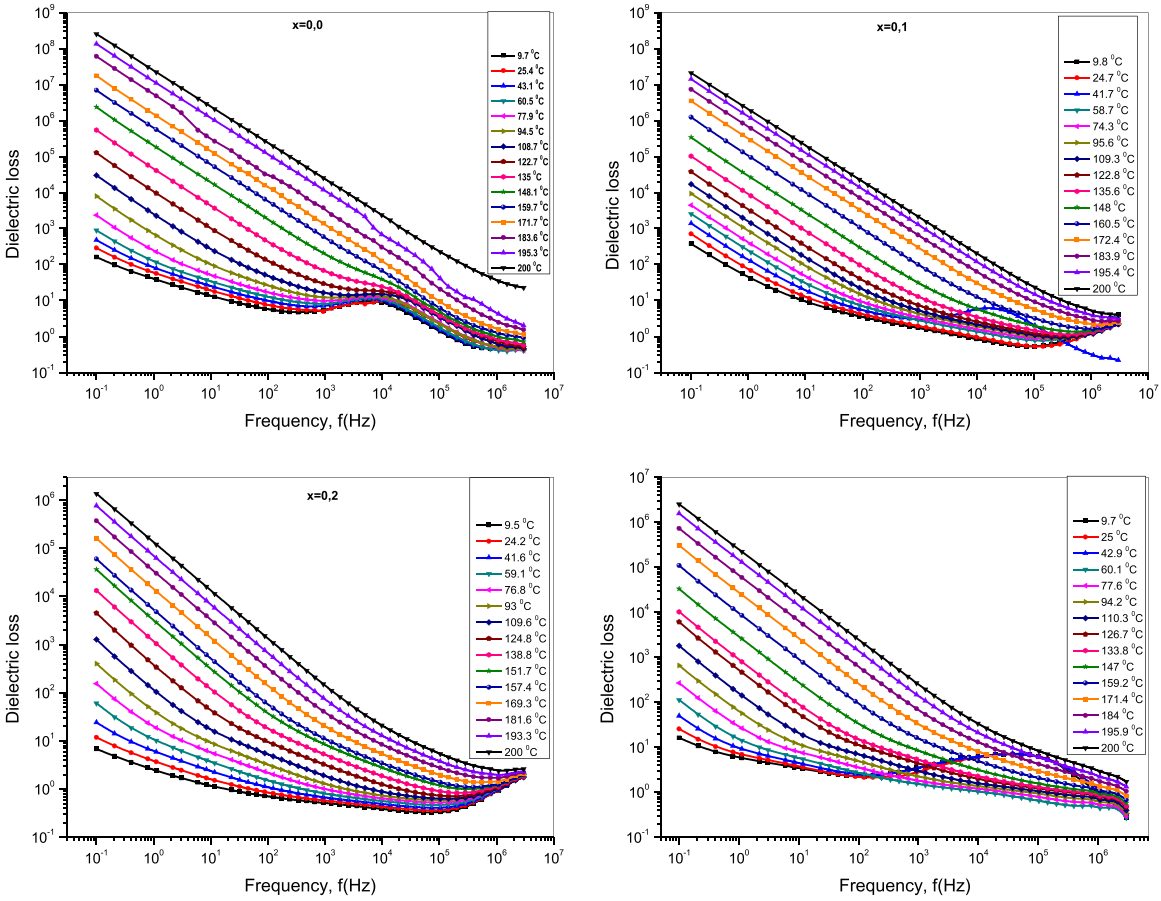

Fig. 9. Dielectric loss of Bi-La-Y substituted SrM ($0.0 \leq x \leq 0.33$) versus frequencies of up to 3 MHz for temperatures ranging from 10 °C to 200 °C.

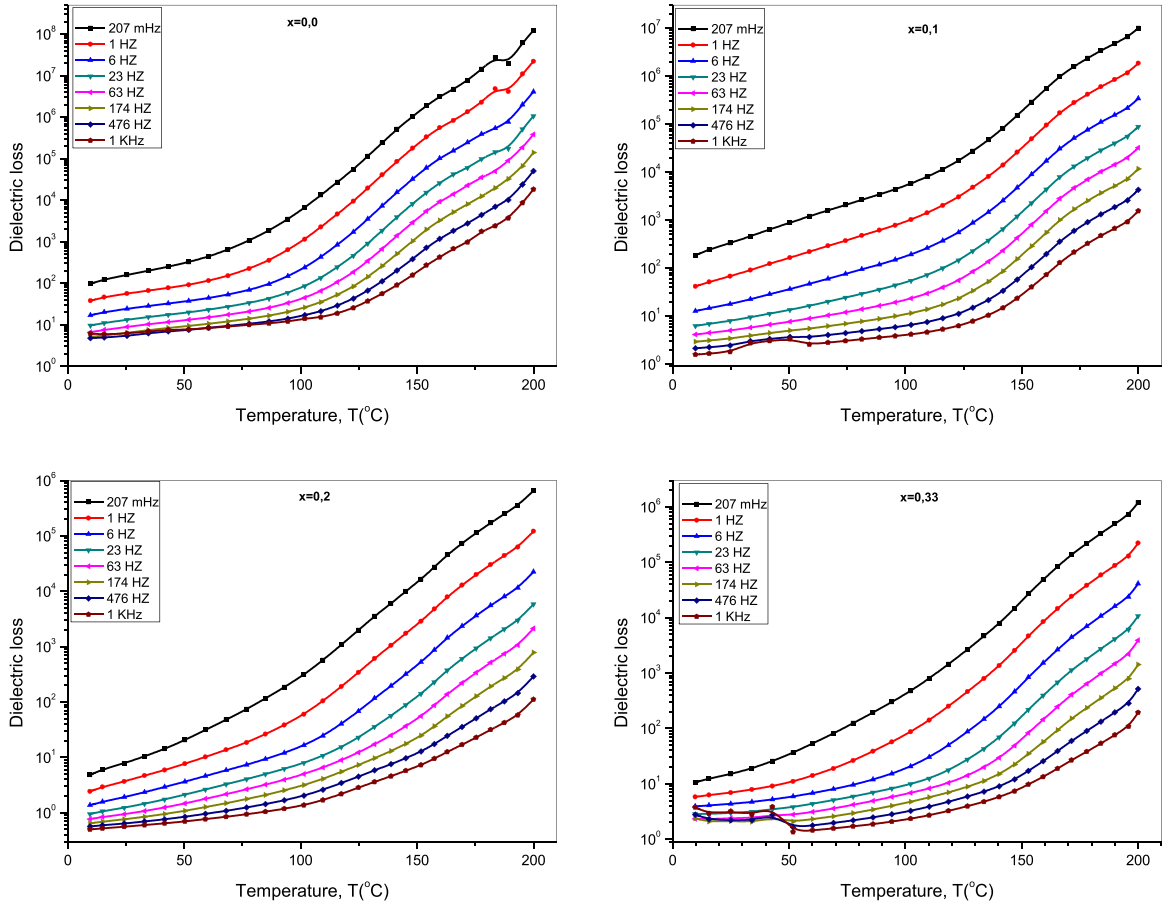

Fig. 10. Dielectric loss of Bi-La-Y substituted SrM ($0.0 \leq x \leq 0.33$) versus temperatures for lower frequencies up to 1 kHz.

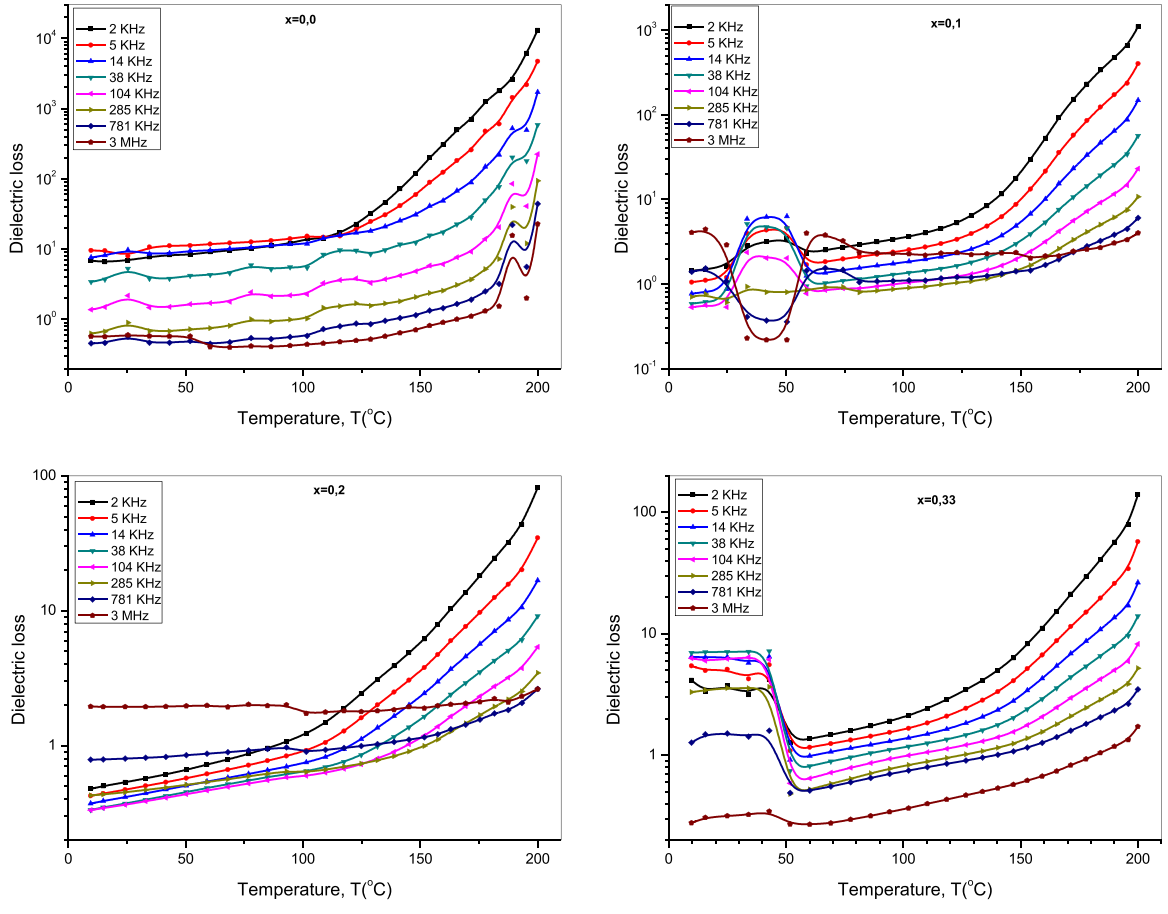

Fig. 11. Dielectric loss of Bi-La-Y substituted SrM ($0.0 \leq x \leq 0.33$) versus temperatures for medium and higher frequencies up to 3 MHz.

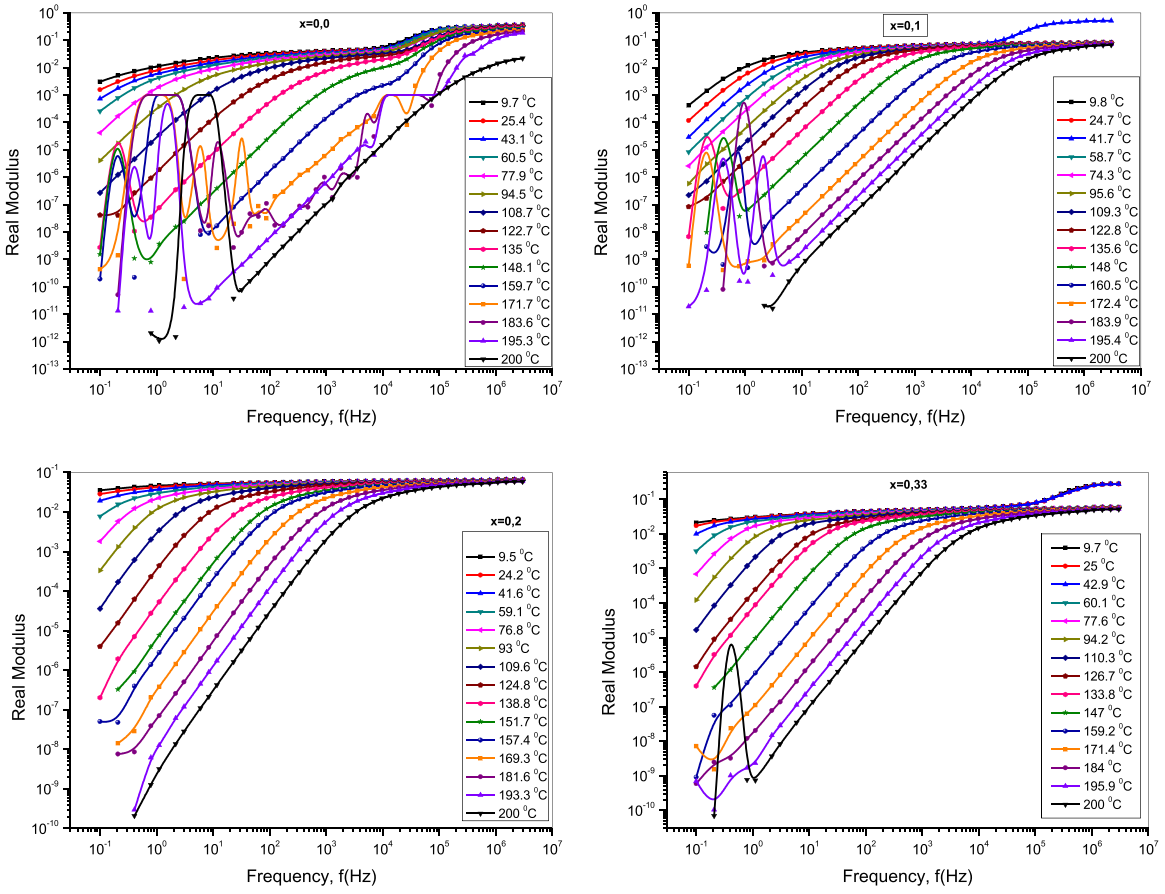

Fig. 12. Real Modulus of Bi-La-Y substituted SrM ($0.0 \leq x \leq 0.33$) versus frequencies of up to 3 MHz for temperatures ranging from 10 °C to 200 °C.

temperature, which suggests that conduction is caused by '*small polaron hopping*' that is diverging from that of the Cr^{3+}-substituted spinel ferrites [35–37]. That is why tendencies of activation energy against substitution of Bi^{3+}, La^{3+} and Y^{3+} ions increase slightly. However, higher activation energy is attributed to the '*electron hopping*' conduction at higher side of temperature as described earlier. The conduction in SrM is considered to occur due to hopping of electrons between Fe^{2+} and Fe^{3+} at octahedral sites. It has been reported that relevant substituents may predominantly occupy octahedral site [33–35]. Due to the replacement of ferric ions by Bi^{3+}, La^{3+} and Y^{3+} ions from the octahedral sites, the number of ferric ions and hence the hopping of electrons decreases.

The increase in *dc* electrical conductivity with Bi, La and Y substitution causes obstruction to the flow of the carriers reducing the accumulation of space charge polarization due to replacement of ferrous and ferric ions from octahedral site. The lossy tangent and dielectric constant therefore would be expected to vary slightly by increasing Bi, La and Y concentration as it has also been proved experimentally.

3.5. Dielectric measurements

3.5.1. Dielectric constant

The measurement of dielectric parameters (dielectric constant, dielectric loss and dielectric loss factor) provides useful information about the behavior of electric charge carriers which is helpful in understanding the conduction mechanism of ferrites. Dielectric constant of Bi-La-Y substituted SrM versus frequencies of up to 3 MHz is shown in Fig. 6 for temperatures ranging from 10 °C up to 200 °C. In a specific case of Figs. 6–8, the dielectric constant of non-substituted hexaferrites is seen to be fluctuated at a higher temperature range over 150 °C for the dominated lower, medium and less effective higher frequencies. It is also noted that the magnitude of dielectric constant is effectively saturated in a certain range. The fluctuation of dielectric constant seems to be in the form of inversely one or more peaks as a reduction at a certain temperature for a range of frequencies.

In general, dielectric constant decreases with frequencies up to a range of 3.0 MHz while it increases with temperature especially more obvious for $x=0.2$ in which its variation is regulated and seems to be more clear to understand the conduction mechanisms of the complicated Bi-La-Y substituted SrM.

Once again, dielectric constant of Bi-La-Y substituted SrM versus temperatures is shown in Fig. 7 for lower frequencies up to 1.0 kHz and in Fig. 8 for medium and higher frequencies up to 3.0 MHz. As can be seen from both set of the graphs for all the substitution up to 0.33, the dielectric constants as function of temperature for both frequency regions have some different tendencies. These can be attributed to a conduction contribution of both electron and polaron hopping mechanism. Because of the complexity of studied hexaferrites, the dielectric constant relies on how speedy the level of polarization organizes itself to keep up with the oscillations of an externally-applied electric field. Being increased the frequency, the polarization orientation declines because the alignment of dipole moments requires a longer time interval than electronic and ionic polarizations, which give rise to a reduction in dielectric constant, and the reduction rate is nearly differing for all the samples in dependence with temperature, frequency and the ratio of substitutions. The variation of relative dielectric constant with frequency discloses the presence of electrode interface polarization processes, which appears at lower

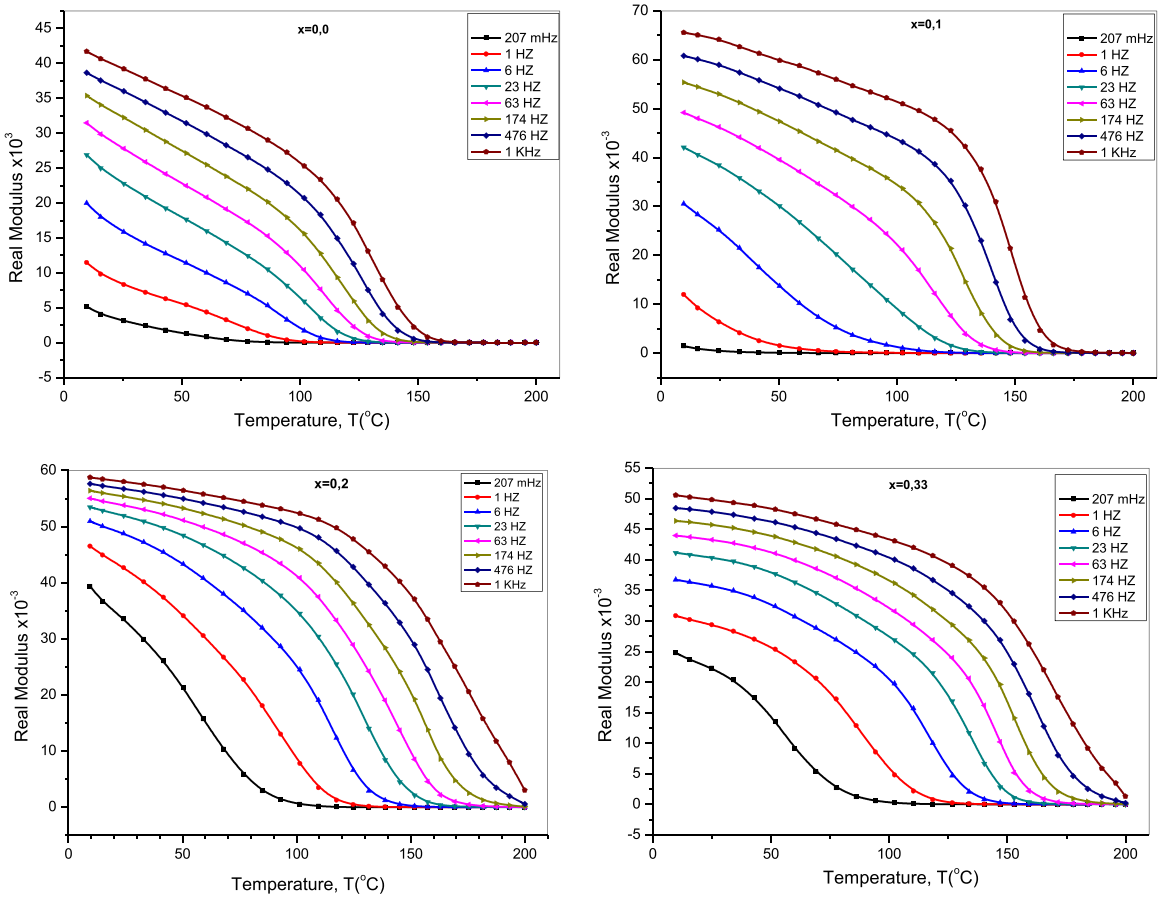

Fig. 13. Real Modulus of Bi-La-Y substituted SrM ($0.0 \leq x \leq 0.33$) versus temperatures for lower frequencies up to 1 kHz.

frequencies. With regard to the temperature dependency, the dielectric constant, in general, increases with temperature attributable to the molecular orientation and arrangement [38]. Consequently, dielectric constant of $SrLa_xBi_xY_xFe_{12-3x}O_{19}$ ($0.0 \leq x \leq 0.33$) increases with the increase of temperature because of the improvement of boundaries between Bi-La-Y substitutions and strontium ferrites by changing compositional ratios of Bi-La-Y against Sr in $Sr\text{-}Bi_xLa_xY_xFe_{12-3x}O_{19}$.

The value of dielectric constant varies with increasing Bi-La-Y substitution. As it has already discussed that Bi^{3+} oxidizes to Bi^{5+} which occupies the tetrahedral sites increasing the concentration of ferrous ions as well as the charge transfer between ferrous and ferric ions at octahedral site which increases the charge polarization. The value of dielectric constant is therefore expected to vary with increasing Bi-La-Y substitution. The electrical data is in good agreement with the dielectric constant data.

It should be also emphasized that the rise in thermal energy yields substantial enhancement of mobility of the charge carriers. It is highlighted that the measured effective permittivity depends both on the microstructure and on the permittivity of compositions [39]. So, this micro structural condition could be explained by Clausius–Mosotti equation [40], which clarifies the relationship between dielectric constant of a substance and polarizability coefficient of its dipoles. Therefore, the decline in polarization effect with decreasing temperature instigates a slightly drop in dielectric constants of the SrM as shown in Figs. 6–8.

The resonance behavior in dielectric constant is observed in some values of frequencies and temperatures. The peaks observed in these values are due to resonance of frequencies of hopping with that of externally applied electric field. As the polarization mechanism in ferrites is due to exchange of electrons between ferrous and ferric ions at octahedral sites, when the hopping frequency between ferrous and ferric ions matches with that of externally applied electric field maximum loss is observed. The decrease in the value of dielectric constant with increase in frequency is a normal behavior of ferrites which is observed by various other researchers [41,42].

3.5.2. *Dielectric loss*

Dielectric loss of Bi-La-Y substituted SrM versus frequencies of up to 3 MHz for temperatures ranging from 10 °C to 200 °C is given in Fig. 9 for a four different substitutions of $x=0.0$; 0.1; 0.2 and 0.33. Non-substituted hexaferrites shows a shoulder at lower temperature in the range of slightly higher frequency at about 10 kHz while it disappears for higher temperatures. Moreover, it is interesting to note that especially for a temperature of 40 °C a shoulder takes place for substitutions of 0.1 and 0.33 except for 0.2.

As a general view, the dielectric loss for substituted and non-substituted strontium hexaferrites shows a power law tendency i.e. a linear drop in the *log-log* plots. Its temperature and frequency dependency display a highly linear decrease with frequency at low frequency regime, which is more significant at higher temperatures, on the contrary this curves gives us a variety of tendencies at higher frequencies depending upon ratios of the Bi-La-Y ions. This linearity part at the lower frequencies of the log-log graph corresponds to the power law with an exponent, which is described by the following equation;

$$\varepsilon''(\omega;\, T) = \varepsilon''(0;\, T)\omega^n \tag{8}$$

where ω is the angular frequency and $\varepsilon''(0;T)$ is the pre-coefficient dielectric loss which is depended strongly on temperatures as

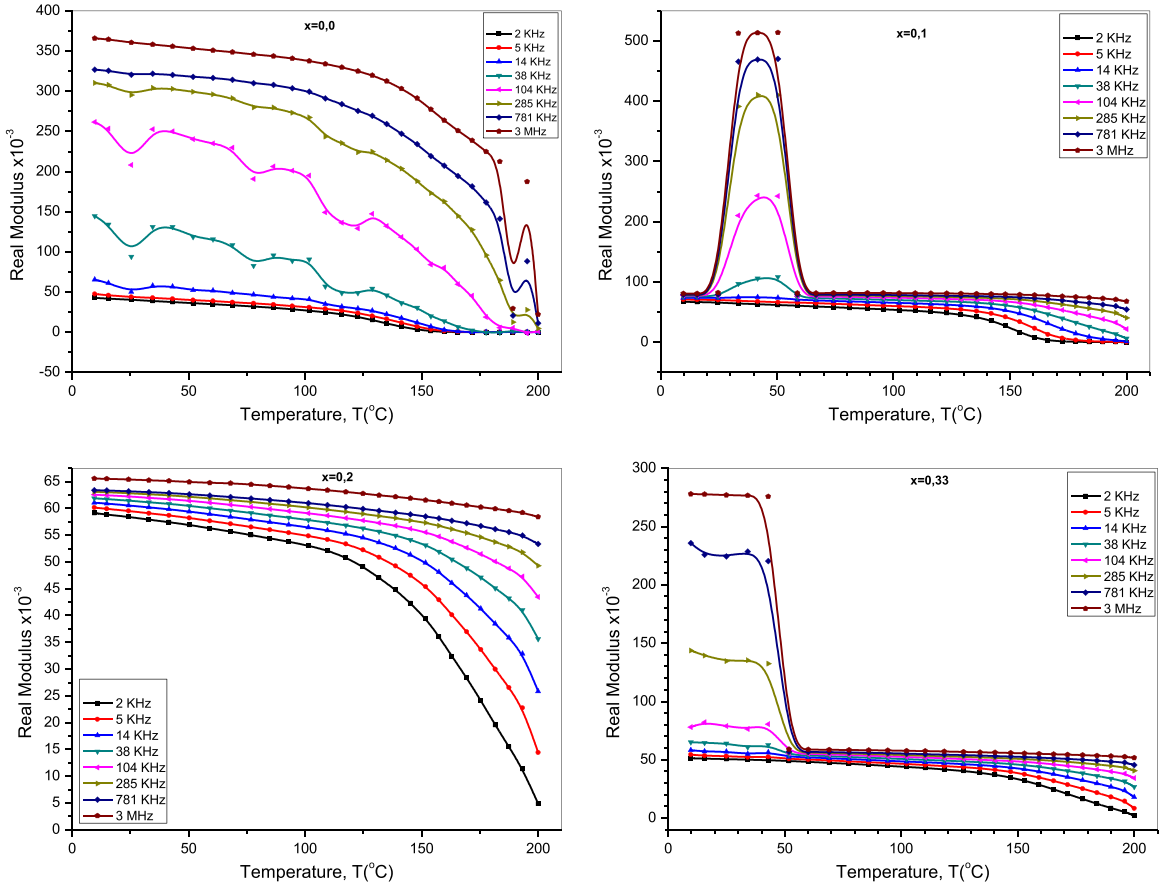

Fig. 14. Real Modulus of Bi-La-Y substituted SrM ($0.0 \leq x \leq 0.33$) versus temperatures for medium and higher frequencies up to 3 MHz.

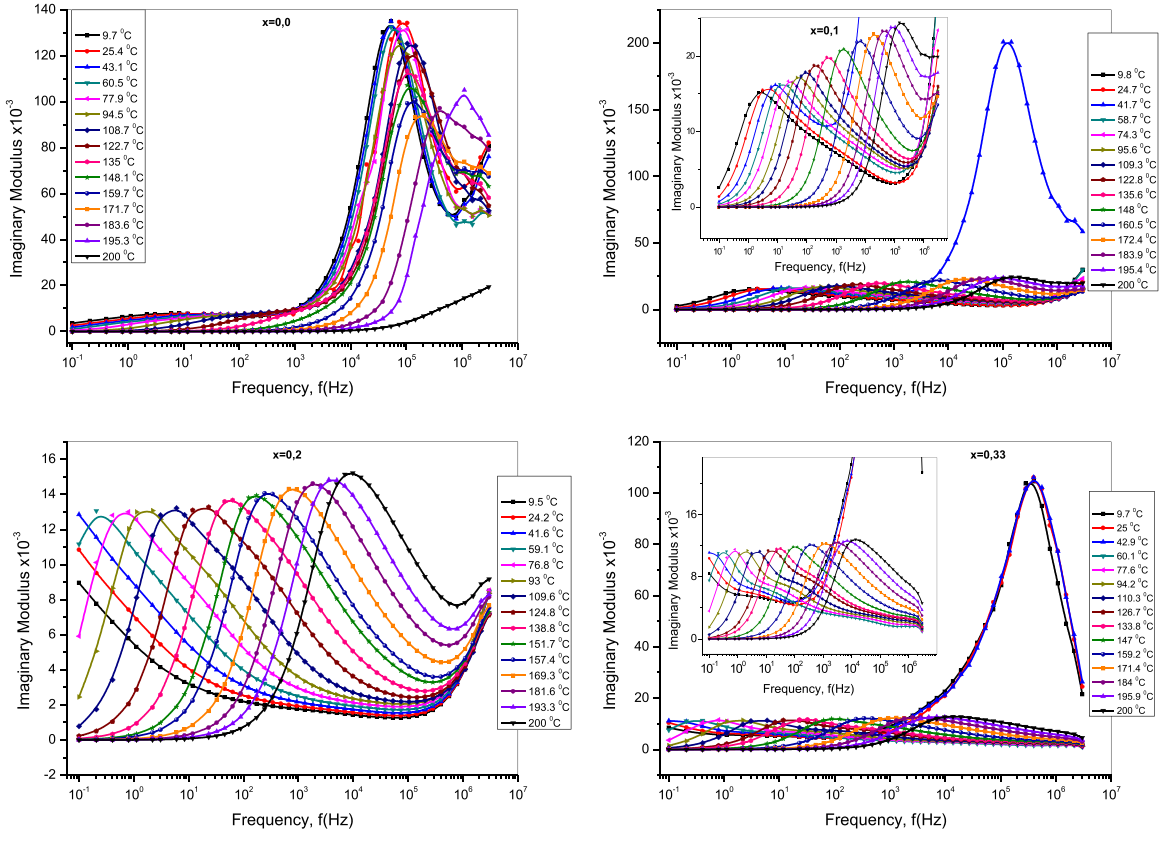

Fig. 15. Imaginary Modulus of Bi-La-Y substituted SrM ($0.0 \leq x \leq 0.33$) versus frequencies of up to 3 MHz for temperatures ranging from 10 °C to 200 °C.

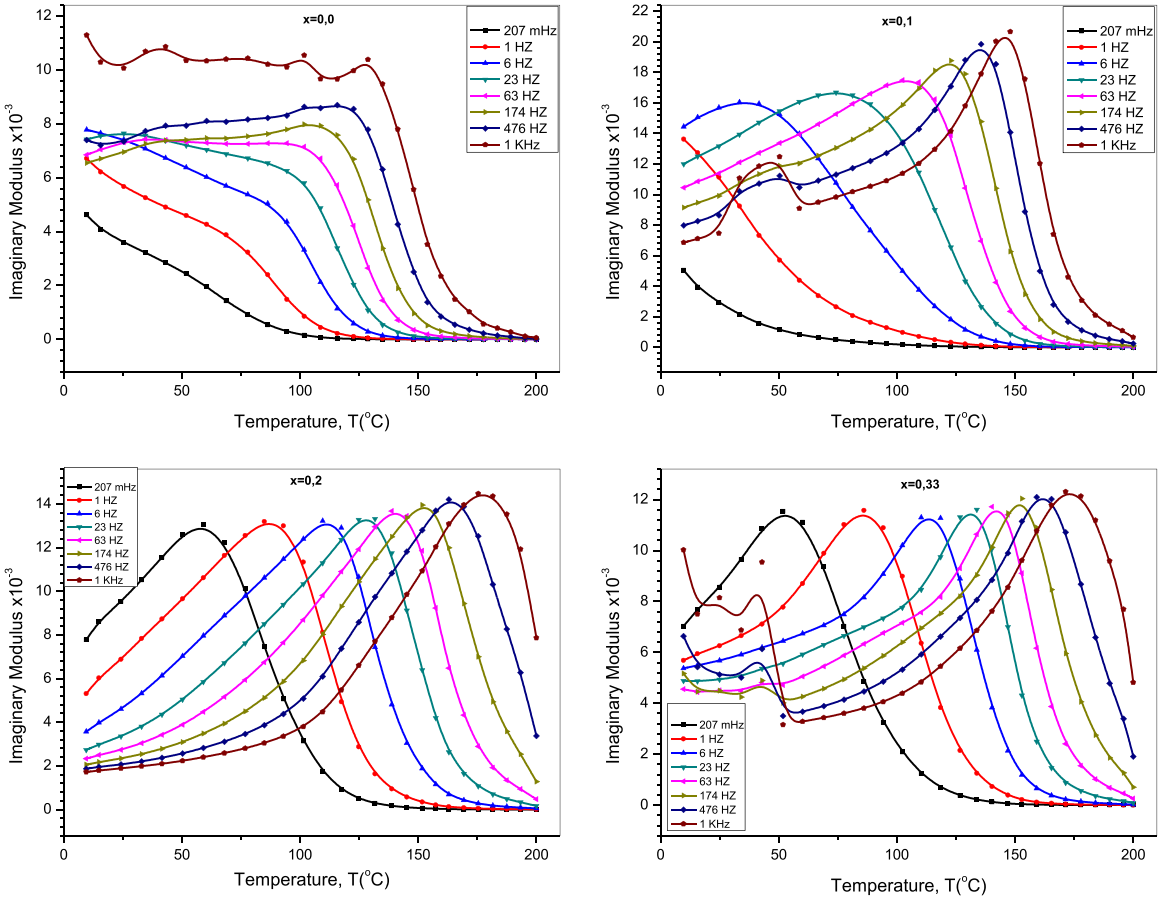

Fig. 16. Imaginary Modulus of Bi-La-Y substituted SrM ($0.0 \leq x \leq 0.33$) versus temperatures for lower frequencies up to 1 kHz.

shown in Figs. 10 and 11. '*n*' is the power exponent correlated with the temperatures and substitution of Ba-La-Y ions in Sr-hexaferrites and also Sr-hexaferrites itself as illustrated with Figs. 9–11. It can be therefore, considered that the conduction mechanism depends both on temperature and on the nature of the reorganization owing to the structural diffusion among the elemental compositions. It is also obvious to notice that the capacitive response of the particles exhibits more temperature dependent behavior rather nature of the reorganization of Bi-La-Y substituted SrM. This linearity part at the lower frequencies of the log-log graph corresponds to the dc conductance (σ_{dc}), which can be expressed as by the following equation;

$$\varepsilon''_{dc} = \sigma_{dc}(\omega C_o \tag{9}$$

where C_o is the vacuum capacitance. The reduction of dielectric loss ultimately reaches a minimum at a higher frequency and shifts to higher frequency side in general depending upon the ratio of *substitution* ions in SrM. According to the phenomenological theory, the dielectric structure of a ferrite seems to be classified into two layers. First layer consists of large ferrite grains and behaves like a conducting layer [10]. Second one comprises grain boundaries which are poor conductors. Due to transfer of electrons between ferrous and ferric ions, the limited drift motion of electrons occurs in the direction of externally-applied field which establishes the polarization. The level of polarization diminishes with increasing frequency because at high-frequency of external field, the electronic transferring between ferrous and ferric ions delays behind the alternating field. Since the synthesized samples include small crystallite size than bulk material, then, they contain more grain boundaries. As the samples comprise large number of grain boundaries than the bulk material which are poor conductors it gives rise to low value of dielectric constant.

The decrease in the values of both dielectric constant and lossy tangent with the frequency is a normal behavior for ferrites and can be explained on the basis of charge polarization. The charge polarization is a result of the existence of higher conductivity phase (*grains*) in the insulating matrix (*grain boundaries*) of a dielectric, causing localized accumulation of charge under the stimulus of external electric field. The reduction in the dielectric constant and lossy tangent occurs since the frequency of hopping of electron exchange between ferric and ferrous ions is far from the frequency of the externally applied alternating electric field. It is important to note that there is a strong relationship between the conduction and the polarization mechanism (dielectric constant) [43]. The space charge polarization appears attributable to the electron displacement when electric field is applied across the sample. The consequential charge developed at the insulating grain boundary acts as a major contributor to the dielectric constant in hexaferrites. Therefore, increasing the number of ferrous ions at octahedral site the space charge polarization is supposed to be enhanced due to the ease of electron transfer between ferrous and ferric ions and as a result the dielectric constant would have higher values.

3.5.3. *Dielectric modulus*

The dielectric modulus can be divided into both real and imaginary components of complex dielectric data relevant to dielectric constant ε' and and dielectric loss ε'' and then is expressed in the form of [44,45];

$$M^* = \frac{1}{\varepsilon^*} = M' + iM'' = \frac{\varepsilon' + i\varepsilon''}{\varepsilon'^2 + \varepsilon''^2} \tag{10}$$

where M' and M'' is the real and complex component of

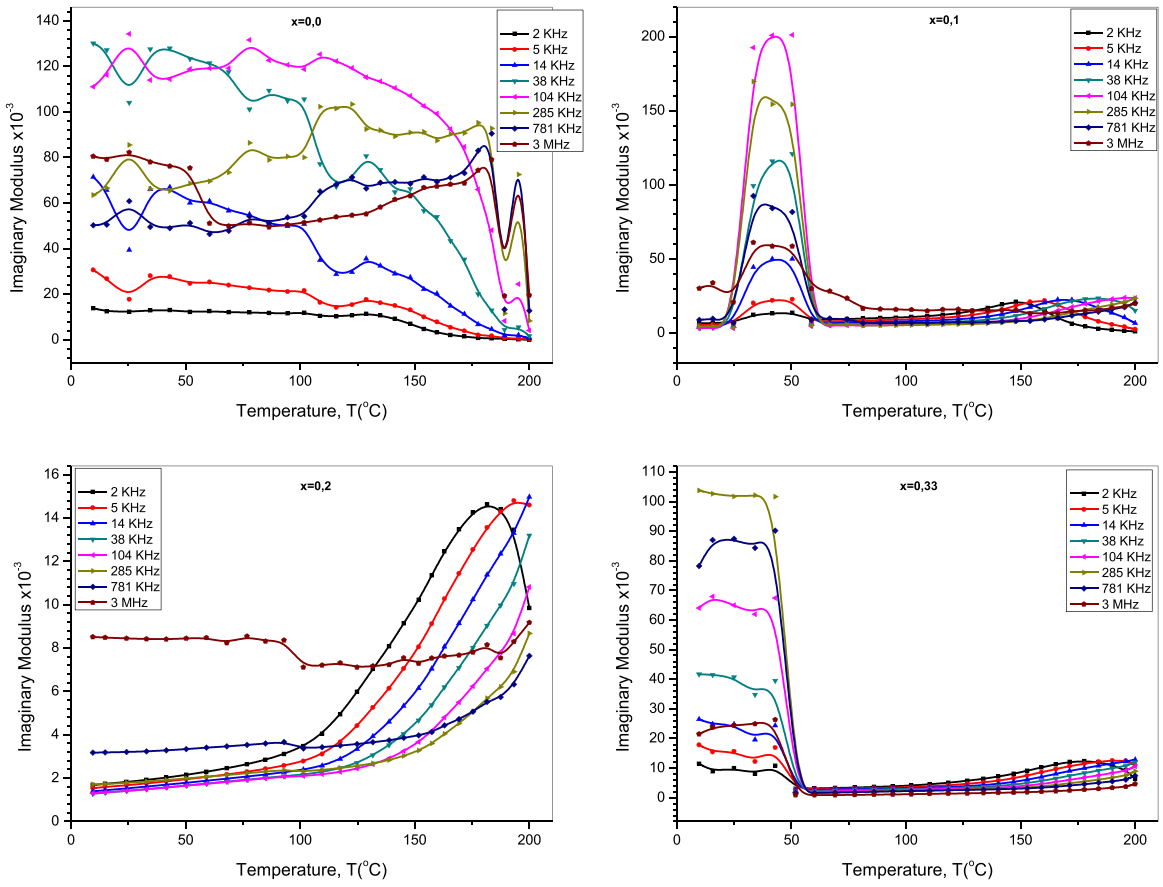

Fig. 17. Imaginary Modulus of Bi-La-Y substituted SrM ($0.0 \leq x \leq 0.33$) versus temperatures for medium and higher frequencies up to 3 MHz.

dielectric modulus respectively.

Real Modulus of Bi-La-Y substituted strontium SrM versus frequencies of up to 3 MHz for temperatures ranging from 10 °C to 200 °C is summarized in the form of graphs in Fig. 12. It is evident to emphasized that real modulus increases with increasing with frequencies obeying some kind of power law. It is also note that at higher frequency and some peaks in real modulus is observed for higher temperatures except for $x=0.2$. clearly seen from the graphs. At lower temperature the real modulus represents less variation in magnitude while high temperature shows quite a huge variation, especially lower frequencies. However, it is almost independent to the temperatures for higher frequencies in general which means the curves are saturated, in which saturation and dependency is also relevant to the substitutions.

Real Modulus of Bi-La-Y substituted SrM versus temperatures for lower frequencies up to 1 kHz is represented in Fig. 13. It is note that real modulus reduces with increasing temperatures but increases with frequency at lower temperature while it is minimized at higher temperature in which saturation is shifted to higher temperature.

Real Modulus of Bi-La-Y substituted SrM versus temperatures for medium and higher frequencies up to 3 MHz from 2 kHz is shown in Fig. 14. As can be seen from the four graphs of all the substitutions, it is not easy to understand what happens to the electrical mechanism for all of them. Here non-substituted SrM represents that real modulus at higher frequency range decreases with increasing temperatures but increases tremendously with increasing frequencies as a peak occurs at around 195 °C over a frequency of 250 kHz. For $x=0.1$, a resonance peak takes place at about a temperature of 40 °C and increases with increasing frequencies of over 35 kHz. Then it decreases slightly with decreasing temperatures for the reduction influences of increasing frequencies. For the case of $x=0.2$, real modulus reduces with increasing temperatures however, the increase of frequency reduces the level of variation in real modulus. Final option in the case of $x=0.33$ depicts the different attitudes. It shows a similar variation as in the case of $x=0.1$ however, expanded peaks occurs below a temperature of around 50 °C for higher frequencies over 35 kHz again.

Imaginary modulus of Bi-La-Y substituted SrM versus frequencies of up to 3 MHz is shown in Fig. 15 for temperatures ranging from 10 °C to 200 °C. for SrM, the imaginary modulus increases slightly with frequency up to 1 kHz and then suddenly increases sharply but and peak occurs with a shift to the higher frequency side. For the case of $x=0.1$, imaginary modulus has a peak value which shifts to the higher frequency side with an elevated temperature. It is also note that a huge peak of temperature of 41.7 °C is resonated at a frequency of around 100 kHz as shown in the graph. Similar tendencies can be observed for the $x=0.33$ as in the case of $x=0.1$. Only differences in resonance peaks can be recorded for some higher temperature values over 160 °C together with a shift to a frequency of 800 kHz. For a substitution of $x=0.2$, the resonance peak value of imaginary modulus is shifted to a higher frequency side while the temperature is increased regularly up to 200 °C.

Imaginary modulus of Bi-La-Y substituted SrM versus temperatures for lower frequencies up to 1 kHz is depicted in Fig. 16. For a SrM, the imaginary modulus is decreased and diminishes for lower frequencies. For 500 Hz and 1 kHz, it increases and fluctuates up to a certain value and decreases suddenly. For Bi-La-Y substituted SrM it increases generally, and generates a peak value, and then decreases and also shifts steadily with increasing temperatures.

Imaginary modulus of Bi-La-Y substituted SrM versus

temperatures for medium and higher frequencies up to 3 MHz is shown in Fig. 17. For SrM, it fluctuates while decreasing with temperatures and a peak occurs at a temperature of about 195 °C over a frequency of 250 kHz. For x=0.1, a resonance peak takes place at about a temperature of 40 °C and increases with increasing frequencies of over 2 kHz. Then it decreases slightly with decreasing temperatures for the reduction influences of increasing frequencies. For the case of x=0.2, imaginary modulus increases with increasing temperatures however, the increase of frequency reduces the level of variation in imaginary modulus, especially for frequencies over 750 kHz. Final option in the case of x=0.33 depicts the different attitudes as in the case of real one. It shows a similar variation as in the case of $x=0.1$ however, expanded peaks occurs below a temperature of around 50 °C for higher frequencies over 2 kHz again.

4. Conclusion

The influences of Bi, La and Y ions of SrM on ac/dc conductivities, dielectric constant/loss properties as well as complex dielectric modulus were investigated extensively for a variety of substitution. AC conductivity increases with increasing frequency which could be considered as an origin indication of both electron and polaron hopping mechanisms. It is also worthy to note that the activation energy is increased as the enhanced contributions of substitutions in SrM with the illustration of a better stability and tunability of electrical bonds among substitutional ions and, ferrous and ferric ions. So this would be an indication of both mechanisms-individual and combinational contributions- mentioned above, depicted in the Arrhenius plot. The dielectric constant, dielectric loss and dielectric modulus represent a very interesting value of tunability and optimised consequences regarding to the variation of frequencies, temperatures and selected ratios of substitutions in SrM. The improvement in the electrical conductivity and the decrease in both dielectric constant and loss make the synthesized materials suitable for the application in microwave devices because a high resistivity material is required for the applications in microwave devices.

Acknowledgements

The authors would like to thank Fatih University (P50031504_B (10790)) and Namık Kemal University (NKUBAP.06. GA.16.047).

References

[1] R. Dehghan, S.A. Seyyed Ebrahimi, Optimized nanocrystalline strontium hexaferrite prepared by applying a methane GTR process on a conventionally synthesized powder, J. Magn. Magn. Mater. 368 (2014) 234–239.
[2] X. Tang, R.Y. Hong, W.G. Feng, D. Badami, Ethylene glycol assisted hydrothermal synthesis of strontium hexaferrite nanoparticles as precursor of magnetic fluid, J. Alloy. Compd. 562 (2013) 211–218.
[3] H. Sözeri, A. Baykal, B. Ünal, Low-temperature synthesis of single-domain Sr-hexaferrite particles by solid-state reaction route, Phys. Status Solidi (A) 209 (2012) 2002–2013.
[4] S.M. Masoudpanah, S.A. Seyyed Ebrahimi, C.K. Ong, Magnetic properties of strontium hexaferrite films prepared by pulsed laser deposition, J. Magn. Magn. Mater. 324 (2012) 2654–2658.
[5] R.C. Pullar, Hexagonal ferrites: a review of the synthesis, properties and applications of hexaferrite ceramics, Progress Mater. Sci. 57 (2012) 1191–1334.
[6] A. Drmota, M. Drofenik, A. Žnidaršič, Synthesis and characterization of nanocrystalline strontium hexaferrite using the co-precipitation and microemulsion methods with nitrate precursors, Ceram. Int. 38 (2012) 973–979.
[7] S. Chawla, S. Meena, P. Kaur, R. Mudsainiyan, S. Yusuf, Effect of site preferences on structural and magnetic switching properties of Co–Zr doped strontium hexaferrite $SrCo_xZr_x\ Fe_{(12-2x)}O_{19}$, J. Magn. Magn. Mater. 378 (2015) 84–91.
[8] Z. Durmus, H. Kavas, A. Durmus, B. Aktaş, Synthesis and micro-structural characterization of graphene/strontium hexaferrite ($SrFe_{12}O_{19}$) nanocomposites, Mater. Chem. Phys. 163 (2015) 439–445.
[9] I.A. Auwal, H. Güngüneş, A. Baykal, S. Güner, S.E. Shirsath, M. Sertkol, Structural, morphological, optical, cation distribution and Mössbauer analysis of Bi^{3+} substituted strontium hexaferrite, Ceram. Int. 42 (2016) 8627–8635.
[10] I.A. Auwal, B. Ünal, H. Güngüneş, S.E. Shirsath, A. Baykal, Dielectric properties, cationic distribution calculation and hyperfine interactions of La^{3+} and Bi^{3+} doped strontium hexaferrites, Ceram. Int. 42 (2016) 9100–9115.
[11] C. Koops, On the dispersion of resistivity and dielectric constant of some semiconductors at audiofrequencies, Phys. Rev. 83 (1951) 121.
[12] E. Verwey, J. De Boer, Cation arrangement in a few oxides with crystal structures of the spinel type, Recl. Trav. Chim. Pays-Bas 55 (1936) 531–540.
[13] I. Auwal, A. Baykal, H. Güngüneş, S.E. Shirsath, Structural investigation and hyperfine interactions of $BaBi_xLa_xFe_{12-2x}O_{19}$ ($0.0 \le x \le 0.5$) hexaferrites, Ceram. Int. 42 (2016) 3380–3387.
[14] R.C. Alange, P.P. Khirade, S.D. Birajdar, A.V. Humbe, K.M. Jadhav, Structural, magnetic and dielectrical properties of Al–Cr Co-substituted M-type barium hexaferrite nanoparticles, J. Mol. Struct. 1106 (2016) 460–467.
[15] M. Azim, S. Atiq, S. Riaz, S. Naseem, Phase stablization and frequency dependent dielectric response of La-doped Sr-hexaferrites, Mater. Today: Proc. 2 (2015) 5578–5581.
[16] I.A. Auwal, H. Gungüneş, S. Guner, Sagar E. Shirsath, M. Sertkol, A. Baykal, Structural, magneto-optical properties and cation distribution of $SrBi_xLa_xY_xFe_{12-3x}O_{19}$ ($0.0 \le x \le 0.33$) hexaferrites, Mater. Res. Bull. 80 (2016) 263–272.
[17] J.T.S. Irvine, D.C. Sinclair, A.R. West, Electroceramics: characterization by impedance spectroscopy, Adv. Mater. 2 (3) (1990) 132–138.
[18] A.M. Abo El Ata, M.K. El Nirma, S.M. Attia, D. El Kony, A.H. Al- Hammadi, Studies of AC electrical conductivity and initial magnetic permeability of rare-earth-substituted Li–Co ferrites, J. Magn. Magn. Mater. 297 (2006) 33–43.
[19] B. Unal, Z. Durmus, H. Kavas, A. Baykal, M.S. Toprak, Synthesis, conductivity and dielectric characterization of salicylic acid-Fe_3O_4 nanocomposite, Mater. Chem. Phys. 123 (2010) 184–190.
[20] B. Ünal, A. Baykal, Effect of Zn substitution on electrical properties of nanocrystalline cobalt ferrite, J. Supercond. Nov. Magn. 27 (2014) 469–479.
[21] M.J. Iqbal, M.N. Ashiq, P.H. Gomez, Effect of doping of Zr–Zn binary mixtures on structural, electrical and magnetic properties of Sr-hexaferrite nanoparticles, J. Alloy. Compd. 478 (2009) 736–740.
[22] U.V. Chhaya, R.G. Kulkarni, Metal-insulator type transition in aluminium and chromium co-substituted nickel ferrites, Mater. Lett. 39 (1999) 91–96.
[23] P.B. Belavi, G.N. Chavan, L.R. Naik, R. Somashekar, R.K. Kotnala, Structural, electrical and magnetic properties of cadmium substituted nickel–copper ferrites, Mater. Chem. Phys. 132 (2012) 138–144.
[24] D.A. Vinnik, A.Y. Tarasova, D.A. Zherebtsov, L.S. Mashkovtseva, S.A. Gudkova, S. Nemrava, A.K. Yakushechkina, A.S. Semisalova, L.I. Isaenko, R. Niewa, Cu-substituted barium hexaferrite crystal growth and characterization, Ceram. Int. 41 (2015) 9172–9176.
[25] I. Petrila, F. Tudorache, Influence of partial substitution of Fe^{3+} with W^{3+} on the microstructure, humidity sensitivity, magnetic and electrical properties of barium hexaferrite, Superlattices Microstruct. 70 (2014) 46–53.
[26] N. Kumari, V. Kumarn, S.K. Singh, Synthesis, structural and dielectric properties of Cr^{3+} substituted Fe_3O_4 nano-particles, Ceram. Int. 40 (2014) 12199–12205.
[27] N. Rezlescu, E. Rezlescu, Dielectric porperties of copper containg ferrites, Phys. Status Solidi (A) 23 (1974) 575.
[28] A.M. Abo El Ata, M.A. Ahmed, Dielectric and AC conductivity for $BaCo_{2-x}Cu_xFe_{16}O_{27}$ ferrites, J. Magn. Magn. Mater. 208 (2000) 27–36.
[29] J. Bao, J. Zhou, Z. Yue, L. Li, Z. Gui, Dielectric behavior of Mn-substituted Co_2Z hexaferrites, J. Magn. Magn. Mater. 250 (2002) 131–137.
[30] M.J. Iqbal, M.N. Ashiq, Physical and electrical properties of Zr–Cu substituted strontium hexaferrite nanoparticles synthesized by co-precipitation method, Chem. Eng. J. 136 (2008) 383–389.
[31] E.J.W. Verwey, F. de Boer, J.H. van Santen, Cation arrangement in spinels, J. Chem. Phys. 16 (1948) 1091–1092.
[32] S. Sanghi, A. Agarwal, Rietveld refinement, electrical properties and magnetic characteristics of Ca–Sr substituted barium hexaferrites, J. Alloy. Compd. 513 (2012) 436–444.
[33] C. Venkataraju, G. Satishkumar, K. Sivakumar, Effect of bismuth on the properties of Mn ferrite nanoparticles prepared by co-precipitation method, J. Mater. Sci. Mater. Electron. 23 (2012) 1163–1168.
[34] M. Pal, P. Brahma, D. Chakravorty, Magnetic and electrical properties of nickel-zinc ferrites doped with bismuth oxide, J. Magn. Magn. Mater. 152 (1996) 370–374.
[35] M.K. Fayek, S.S. Ata-Allah, Kh Roumaih, S. Ismail, Thermoelectric power properties of Zn substituted Cu-Ga spinel ferrites, Mater. Lett. 63 (2009) 1010–1012.
[36] S. Verma, J. Chand, M. Singh, Structural and electrical properties of Al^{3+} ions doped nano-crystalline $Mg_{0.2}Mn_{0.5}Ni_{0.3}Al_yFe_{2-y}O_4$ ferrites synthesized by citrate precursor method, J. Alloy. Compd. 587 (2014) 763–770.
[37] M.I. Klinger, Two phase polaron model of conduction in magnetite-like solids, J. Phys. C8 (1975) 3595.

[38] Md Md Amir, B. Ünal, M. Geleri, H. Güngüneş, S.E. Shirsath, A. Baykal, Electrical properties and hyperfine interactions of boron doped Fe_3O_4 nanoparticles, Superlattices Microstruct. 88 (2015) 450–466.
[39] S. Shakoor, M.N. Ashiq, M.A. Malana, A. Mahmood, M.F. Warsi, M. Najam-ul-Haq, N. Karamat, Electrical, dielectric and magnetic characterization of Bi–Cr substituted M-type strontium hexaferrite nanomaterials, J. Magn. Magn. Mater. 362 (2014) 110–114.
[40] T. Honegger, K. Berton, E. Picard et, D. Peyrade, Determination of Clausius–Mossotti factors and surface capacitances for colloidal particles, Appl. Phys. Lett. 98 (18) (2011) 181906.
[41] A.M. Abo El Ata, M.A. Ahmed, J. Magn. Magn. Mater. 208 (2000) 27–36.
[42] J. Bao, J. Zhou, Z. Yue, L. Li, Z. Gui, J. Magn. Magn. Mater. 250 (2002) 131–137.
[43] 18 M.J. Iqbala, M.N. Ashiqa, P. Hernandez-Gomezb, J.M. Munoz, Synthesis, physical, magnetic and electrical properties of Al–Ga substituted co-precipitated nanocrystalline strontium hexaferrite, J. Magn. Magn. Mater. 320 (2008) 881–886.
[44] H. Sözeri, A. Baykal, B. Ünal, Low temperature synthesis of single domain Sr-hexaferrit particles by solid state reaction route, Phys. Status Solidi A 209 (2012) 2002–2013.
[45] A. Baykal, M. Demir, B. Ünal, H. Sözeri, M.S. Toprak, Synthesis, characterization, and dielectric properties of $BaFe_{10}(Mn^{2+}Zn^{2+}Zn^{2+})O_{19}$ hexaferrite, J. Supercond. Nov. Magn. 29 (2016) 199–205.